

# A neuronal PI(3,4,5)P<sub>3</sub>-dependent program of oligodendrocyte precursor recruitment and myelination

Sandra Goebbels<sup>1,8</sup>, Georg L Wieser<sup>1,8</sup>, Alexander Pieper<sup>1</sup>, Sonia Spitzer<sup>2</sup>, Bettina Weege<sup>1</sup>, Kuo Yan<sup>3</sup>, Julia M Edgar<sup>1,4</sup>, Oleksandr Yagensky<sup>1</sup>, Sven P Wichert<sup>1,5</sup>, Amit Agarwal<sup>1</sup>, Khalad Karram<sup>6</sup>, Nicolas Renier<sup>7</sup>, Marc Tessier-Lavigne<sup>7</sup>, Moritz J Rossner<sup>1,5</sup>, Ragnhildur Thóra Káradóttir<sup>2</sup> & Klaus-Armin Nave<sup>1</sup>

**The molecular trigger of CNS myelination is unknown. By targeting *Pten* in cerebellar granule cells and activating the AKT1–mTOR pathway, we increased the caliber of normally unmyelinated axons and the expression of numerous genes encoding regulatory proteins. This led to the expansion of genetically wild-type oligodendrocyte progenitor cells, oligodendrocyte differentiation and *de novo* myelination of parallel fibers. Thus, a neuronal program dependent on the phosphoinositide PI(3,4,5)P<sub>3</sub> is sufficient to trigger all steps of myelination.**

In the peripheral nervous system, the ‘trigger’ of myelination is axon size (> 1 μm), a threshold mediated by Nrg1 type III on the axon surface<sup>1</sup>. Since Nrg1 is not required for CNS myelination<sup>2</sup>, we asked whether axon size can be experimentally increased here by the absence of PTEN (ref. 3), i.e., with phosphatidylinositol-3,4,5-trisphosphate (PI(3,4,5)P<sub>3</sub>) stimulating the AKT1–mTOR pathway (Fig. 1a). To specifically enlarge cerebellar granule cells (GC) and their naturally unmyelinated parallel fiber (Pf) axons, we generated *Tg(mα6)-Cre;Pten<sup>loxP/loxP</sup>* mice<sup>4,5</sup>. Reporter gene expression shows that recombination begins at postnatal day (P) 9 in predominantly postmitotic GC<sup>4</sup>. The cerebellum of *Tg(mα6)-Cre;Pten<sup>loxP/loxP</sup>* mice (hereafter termed *Pten* cKO or ‘mutants’) revealed a loss of *Pten* mRNA (–63%; Fig. 1b) and protein (–80%; *n* = 3 each genotype; *P* = 0.0025, *t* = 6.788, d.f. = 4, two-tailed unpaired Student’s *t*-test; Fig. 1c) compared to *Pten<sup>loxP/loxP</sup>* mice (hereafter termed ‘controls’) at age 3.5 months. Loss of PTEN resulted in enhanced phosphorylation of well-known downstream targets of the PI3K pathway (Fig. 1d).

Mutant mice appeared healthy (Supplementary Video 1), but cerebellar GC layer (GL) and molecular layer (ML) progressively enlarged (Fig. 1e and Supplementary Fig. 1a). Immunostaining of

GABA<sub>A</sub> receptor α6 revealed a gradual size increase of GC somata (Supplementary Fig. 1b). Older mice developed ataxia and tremor (Supplementary Video 2), possibly due to hamartomas at advanced age (Supplementary Fig. 2 and Supplementary Note).

The diameters of Pf axons also increased over time, as quantified by electron microscopy (EM), reaching 0.61 ± 0.009 μm (mean ± s.e.m.) in mutants in comparison to 0.16 ± 0.002 μm in controls at 1 year of age (Fig. 1f,g and Supplementary Fig. 1c). Importantly, radial Pf growth in mutant brains was associated with substantial myelination beginning at age P40 (2.3 ± 0.6% myelinated Pf axons) and progressing over time (3 months: 9.5 ± 1% myelinated Pf axons). At 1 year of age, up to 40 ± 3% of Pf axons were myelinated with an average g-ratio (the ratio between the diameter of the axon itself and the outer diameter of the myelinated fiber) of 0.84. Myelination was visualized by Gallyas silver impregnation (Supplementary Fig. 3a) and anti-CNP immunohistochemistry (Fig. 1h and Supplementary Fig. 3b), including whole-mount immunolabeling combined with light sheet and two-photon microscopy (Supplementary Video 3), as well as EM (Fig. 1i–k). We determined a ‘size threshold’ of approximately 0.25 μm for myelination at all ages tested (Fig. 1k,l). Myelinated Pf axon segments were very rarely seen in controls.

*De novo* myelination included the formation of nodes and paranodes with septate-like junctions (Fig. 1j) and the clustering of Caspr and Nav1.6 on axons (Fig. 1m,n). GC synaptic contacts to Purkinje cell dendrites were restricted to Pf ‘nodal’ regions (Fig. 1o and Supplementary Fig. 4).

The ML normally harbors very few oligodendrocytes and only scattered oligodendrocyte progenitor cells (OPCs), as demonstrated in *Plp1-DsRed;Ng2-EYFP* double-transgenic mice (Fig. 2a). In *Pten* mutants at P45, mature oligodendrocytes were increased in the GL (+33%) and more prominent in the ML (+750%) but unaltered in cerebellar white matter (Fig. 2b). To determine whether OPCs proliferate in the ML or are recruited from the GL, we combined immunostaining with BrdU labeling (Fig. 2c). After 20 d of daily BrdU injections (P25–P45), OPC proliferation (BrdU<sup>+</sup>Olig2<sup>+</sup>) was the same in GL or white matter of mutants and controls (Fig. 2d). However, OPC proliferation in the mutant ML increased 4.4-fold. Even at age 6–7 months, we found a 4.7-fold increase of BrdU<sup>+</sup>Olig2<sup>+</sup> cells. This suggests that local proliferation was stimulated (directly or indirectly) by GC axon-derived signals, which must still have been present at older ages. At that time, oligodendrocyte lineage cells in mutants were increased tenfold over the numbers present in controls (Fig. 2d). By following different BrdU protocols, we identified a time window (P20–P30) in which proliferation of OPCs was already increased but the number of CNP<sup>+</sup> oligodendrocytes was not yet altered (Fig. 2e,f). This strongly suggests that OPC proliferation was not merely a homeostatic mechanism

<sup>1</sup>Department of Neurogenetics, Max Planck Institute of Experimental Medicine, Göttingen, Germany. <sup>2</sup>Wellcome Trust-MRC Stem Cell Institute, Cambridge Centre for Brain Repair, and Department of Veterinary Medicine, University of Cambridge, UK. <sup>3</sup>Charité–Universitätsmedizin Berlin, Institute of Cell Biology and Neurobiology, NeuroCure Cluster of Excellence, Berlin, Germany. <sup>4</sup>Present address: Institute of Infection, Immunity and Inflammation, University of Glasgow, UK. <sup>5</sup>Present address: Department of Psychiatry, Ludwig-Maximilians-Universität, München, Germany. <sup>6</sup>Universitätsmedizin Mainz, Institute for Molecular Medicine, Mainz, Germany. <sup>7</sup>Laboratory of Brain Development and Repair, The Rockefeller University, New York, USA. <sup>8</sup>These authors contributed equally to this work. Correspondence should be addressed to S.G. (sgoebbels@em.mpg.de) or K.-A.N. (nave@em.mpg.de).

Received 5 July; accepted 26 September; published online 24 October 2016; doi:10.1038/nn.4425

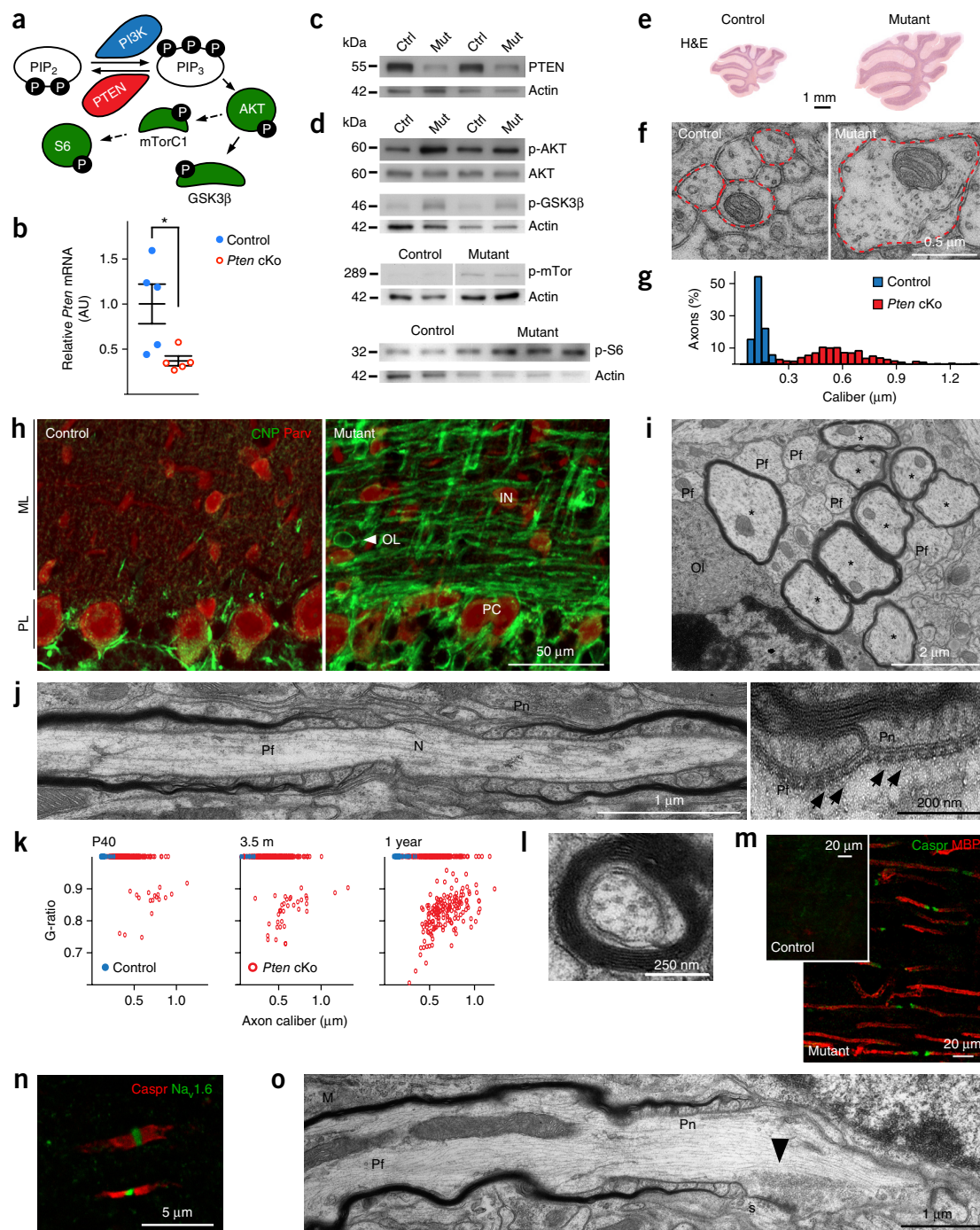


**Figure 1** *Pten* mutant GC trigger *de novo* myelination of Pf axons. (a) Schematic representation of selected candidates of PI3K–AKT1–mTORC1 signaling. (b) Reverse-transcription quantitative real-time PCR (RT-qPCR) shows that *Pten* transcripts containing the *loxP*-flanked exon 5 are decreased in the cerebellum of *Pten* cKO mutants (age 3.5 months). Data show mean  $\pm$  s.e.m.;  $n = 5$  mice per genotype ( $P = 0.0231$ ,  $t = 2.803$ , d.f. = 8, two-tailed unpaired Student's *t*-test). (c) On western blots PTEN levels are decreased in the cerebellum of mutants (age 3.5 months, cropped blot images). (d) Phosphorylation (p-) of the PI3K downstream effectors AKT1, GSK3 $\beta$ , mTOR and S6 is enhanced in *Pten* mutant mice (age 3.5 months, cropped blot images). (e) Conditional ablation of *Pten* in GC causes cerebellar enlargement. (f) Pf axons had increased in diameter as shown by EM analysis. (g) Pf axon caliber size distribution ( $n = 3$  mice per genotype; 140 Pf axons quantified per animal). (h) Myelinated Pf axons in the ML of mutant brains (right) immunostained for CNP (green). Purkinje cells (PC) and interneurons (IN) are parvalbumin-positive (red). Arrowhead, oligodendrocyte (OL) cell body. PC, Purkinje cell layer. (i) Normally unmyelinated Pf axons become *de novo* myelinated in mutant mice (asterisks). (j) Formation of a node of Ranvier (N), flanked by paranodal myelin loops (Pn; left panel) and septate-like junctions (right panel) with the Pf membrane at the EM level. (k) Progressive myelination quantified by g-ratio analysis at the indicated ages (g = 1.0 denotes unmyelinated axons,  $n = 3$  mice per age and genotype, 140 Pf axons quantified per animal). (l) *De novo* myelination of Pf axons requires a minimum axonal caliber of 0.25  $\mu$ m. (m,n) Myelination of Pf axons includes the clustering of axonal Caspr (m, green) and Na $v$ 1.6 (n, red) at newly formed nodes. (o) Myelinated Pf axon synapsing on a Purkinje cell dendritic spine. En passant synapse with presynaptic vesicles (arrowhead) is restricted to newly established node. M, myelin; s, dendritic spine. e–j and l–o, age 1 year. Images in e, f, h–j and l–o are representative of  $\geq 3$  similar experiments. Full-length blots are provided in **Supplementary Figure 13**.

to replace differentiated OPCs but was an early response to the neuronal trigger. Accordingly, BrdU<sup>+</sup>Olig2<sup>+</sup> OPCs were uniformly distributed in the ML and not preferentially detected in proximity to newly generated MBP<sup>+</sup> oligodendrocytes (Fig. 2g).

Double-labeling for BrdU and carbonic anhydrase II (CAII), a marker of mature oligodendrocytes, confirmed that newly generated OPCs had responded to elevated differentiation signals (Fig. 2h). At 7 months, the ML in *Pten*-mutant brains still contained ‘maturing’

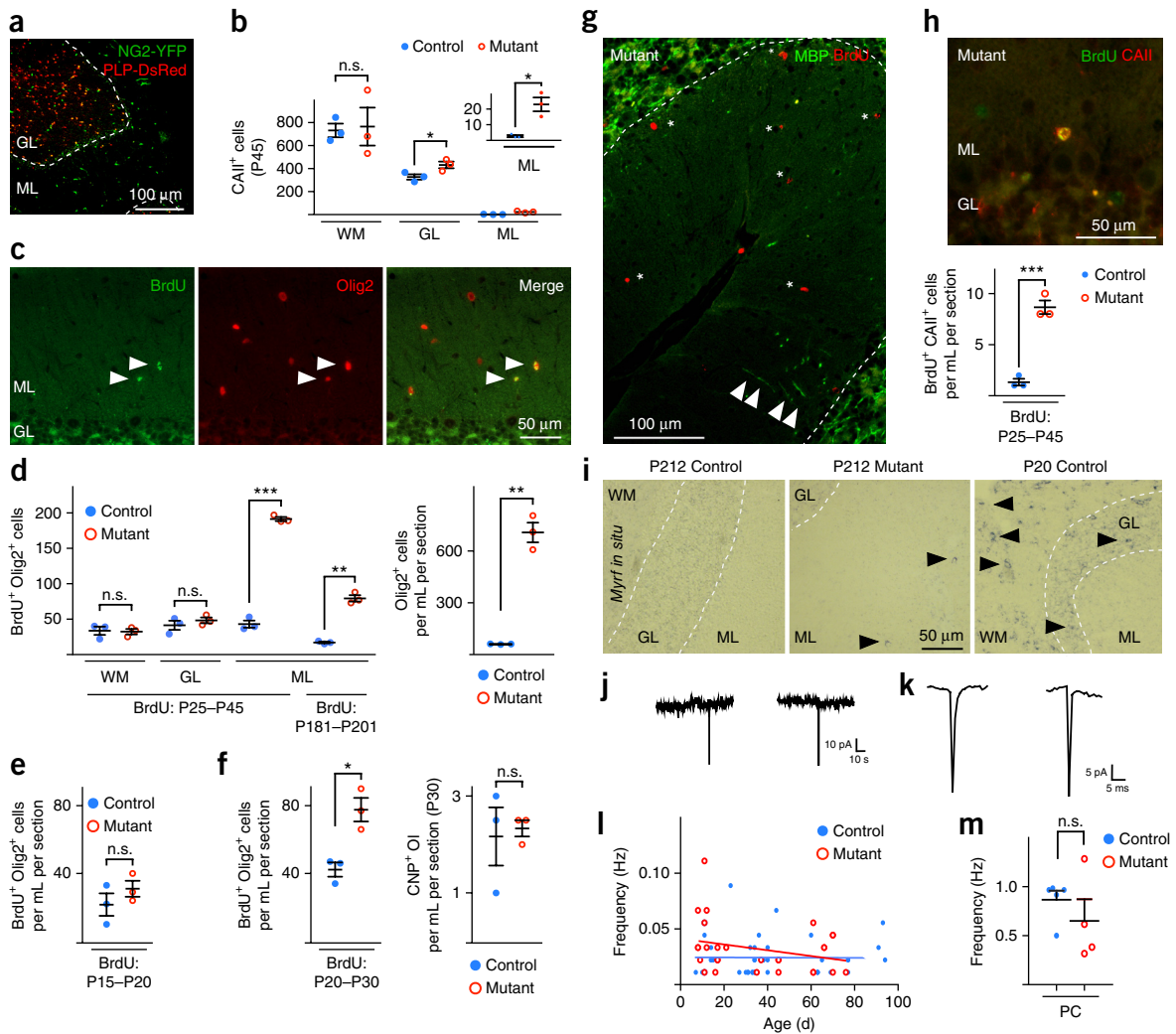


**Figure 2** *Pten* mutant GCs drive OPC proliferation in the ML. (a) Oligodendrocytes (red) are found in cerebellar GL but not in the ML, which contains only scattered NG2<sup>+</sup> OPCs (green). Cells are labeled by DsRed and EYFP fluorescence in double-transgenic *Plp1-DsRed;Ng2-EYFP* mice. (b) Mature oligodendrocytes (CAII<sup>+</sup>) are more numerous in mutant GL ( $P = 0.0498$ ,  $t = 2.780$ , d.f. = 4) and ML ( $P = 0.0103$ ,  $t = 4.562$ , d.f. = 4; inset) but not in white matter (WM;  $P = 0.858$ ,  $t = 0.1907$ , d.f. = 4). Age P45;  $n = 3$  mice per genotype. (c) OPCs in the mutant ML labeled for Olig2<sup>+</sup> (red) and BrdU<sup>+</sup> (green, arrowheads) following daily BrdU administration between P25 and P45 (quantified below). (d) At P45, proliferation of OPCs (BrdU<sup>+</sup>Olig2<sup>+</sup>) is increased in the mutant ML ( $P = 0.0004$ ,  $t = 25.49$ , d.f. = 4) and remains elevated at P201 (following daily BrdU administration between P181 and P201;  $P = 0.0016$ ,  $t = 10.98$ , d.f. = 4). Note that the number of Olig2<sup>+</sup> cells at P201 is tenfold higher in mutants than in controls ( $P = 0.0031$ ,  $t = 11.37$ , d.f. = 4). WM,  $P = 0.8581$ ,  $t = 0.1907$ , d.f. = 4; GL,  $P = 0.4133$ ,  $t = 0.9122$ , d.f. = 4;  $n = 3$  mice per age and genotype. (e, f) Following daily BrdU administration (P15–P20) the number of proliferating OPCs (BrdU<sup>+</sup>Olig2<sup>+</sup>) in ML is similar in mutants and controls (in e;  $P = 0.3161$ ,  $t = 1.145$ , d.f. = 4). While at P30 (and after daily BrdU administration between P20 and P30) the number of proliferating OPCs (BrdU<sup>+</sup>Olig2<sup>+</sup>) in ML is increased in mutants (left panel in f;  $P = 0.0120$ ,  $t = 4.364$ , d.f. = 4), the number of CNP<sup>+</sup> oligodendrocytes (OI) is not (right panel in f,  $P = 0.8025$ ,  $t = 0.2673$ , d.f. = 4).  $n = 3$  mice per genotype and age. (g) Following daily BrdU administration (P25–P45), labeled OPCs (asterisks) distribute evenly and are not preferentially close to newly generated oligodendrocytes and their myelin sheaths (arrowheads). (h) After daily BrdU injections (P25–P45), mature oligodendrocytes can be colabeled for BrdU (green) and CAII (red).  $n = 3$  mice per genotype ( $P = 0.0006$ ,  $t = 9.839$ , d.f. = 4). (i) *In situ* hybridization revealed that *Myrf* mRNA can still be detected in adult *Pten* mutant ML (positive control, wild-type cerebellum at P20). (j) Representative traces of spontaneous postsynaptic inward currents recorded from NG2-EYFP-expressing OPCs clamped at  $-74$  mV in ML of control mice (left) and *Pten* mutant mice (right). (k) Inward currents for control (left) and *Pten* mutant (right) mice at an expanded time scale. (l) Frequency of detectable spontaneous events in OPCs plotted against the age of the animal. The slopes are not significantly different between control (blue,  $n = 42$  cells from 25 animals of 12 different litters) and mutant mice (red,  $n = 28$  cells from 17 animals of 11 litters) ( $P = 0.2$ ,  $F = 1.625$ , d.f. = 66, linear regression). (m) Similarly, we found no significant difference in the frequency of spontaneous inputs in PC, which are predominantly from Pf (control,  $0.9 \pm 0.1$  Hz,  $n = 5$  cells from 2 animals of 1 litter; mutant,  $0.7 \pm 0.2$  Hz,  $n = 4$  cells from 1 animal;  $P = 0.36$ ,  $t = 2.13$ , d.f. = 10). Data are mean  $\pm$  s.e.m.; n.s., not significant. \* $P < 0.05$ ; \*\* $P < 0.01$ ; \*\*\* $P < 0.001$ , two-tailed unpaired Student's *t*-test in b, d, e, f and h; analysis of covariance in l; chi-squared test in (m). Images in a, c and g–i are representative of 3 similar experiments.

oligodendrocytes, as revealed by *in situ* hybridization of *Myrf* mRNA (Fig. 2i), an early marker almost undetectable in fully mature cells (B. Emery, personal communication). Taken together, our data suggest that *Pten*-mutant GC and thus a PI(3,4,5)P<sub>3</sub>-dependent neuronal program is sufficient to drive oligodendrocyte lineage cells through all developmental stages. However, we cannot formally exclude the theoretical possibility that normally myelinated axons recruit OPCs and induce myelination by completely different mechanisms. Formally, activation of neuronal AKT1–mTOR would not be the ‘initiating’ event itself, if other more rate-limiting steps are regulated upstream.

OPCs receive synaptic input that could modulate proliferation and myelination<sup>6</sup>. Using acute slices from mutant and control mice (both additionally expressing an *Ng2-EYFP* transgene<sup>7</sup>), we whole-cell patch-clamped both Purkinje cells, which get input predominantly from Pf axons, and fluorescent OPCs in the ML. This allowed us to determine GC spiking activity as well as the synaptic inputs from Pf axons to OPCs. We found no difference between mutant and control OPCs for the frequency of spontaneous synaptic Pf inputs or for the

Pf inputs to Purkinje cells (Fig. 2j–m). Also, the fraction of OPCs that received detectable input was not different (controls: 39%; mutants: 47%;  $\chi^2 = 0.87$ ,  $P = 0.4$ , chi-squared test). Thus, *de novo* myelination is unlikely to be the result of an underlying alteration of Pf spiking activity or of changes in synaptic input to OPCs (Supplementary Fig. 5 and Supplementary Note).

Theoretically, Pf myelination could be caused by downregulating inhibitory neuronal signals. We addressed this by targeting only a small fraction of sparsely distributed GC, using *Nex-CreERT2* mice<sup>8</sup>. After 5 d of tamoxifen (P10–P15), reporter gene expression marked < 4% of all GC (Supplementary Fig. 6a). However, when analyzed 28 weeks later (Supplementary Fig. 6b), we still found a significant increase of mature oligodendrocytes ( $P < 0.0001$ ,  $t = 19$ , d.f. = 4) and myelinated areas ( $P = 0.009$ ,  $t = 4.730$ , d.f. = 4) in the ML of *Nex-CreERT2;Pten<sup>loxP/loxP</sup>* mice (Supplementary Fig. 6c–f) making it highly unlikely that soluble inhibitors, still expressed by 96% of nonrecombined GC, must be downregulated to initiate myelination. In these mice, *de novo* myelination was also observed when tamoxifen was given at age 7 months (data not shown), arguing strongly against

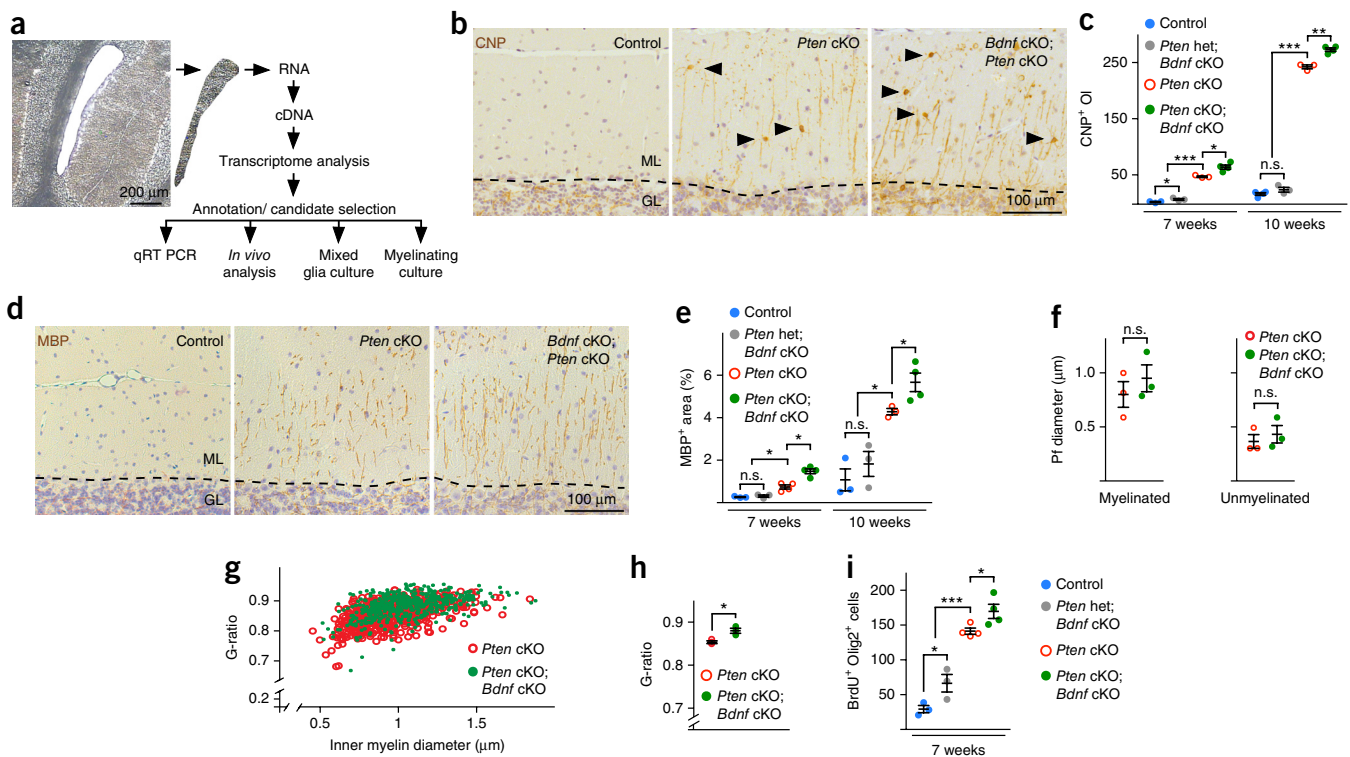


**Figure 3** Screening for candidate promyelinating factors and validation of *Bdnf*. (a) Experimental design to identify and test candidate factors (Supplementary Note) that may regulate oligodendrocyte development in conditional GC-specific *Pten* mutant mice. Laser capture microdissection (LCM) was used to obtain the GL from serial cerebellar sections at age 3 months. (b–e) Double mutants lacking both PTEN and *Bdnf* in GC harbor more CNP<sup>+</sup> oligodendrocytes (OI) in the ML (arrowheads in b, quantified in c: 7 weeks, control vs. *Pten* het; *Bdnf* cKO,  $P = 0.0495$ ,  $t = 2.786$ ; control vs. *Pten* cKO,  $P < 0.0001$ ,  $t = 28.25$ ; *Pten* cKO vs. *Pten* cKO; *Bdnf* cKO,  $P = 0.0132$ ,  $t = 3.757$ , d.f. = 13,  $F = 56.01$ ; 10 weeks, control vs. *Pten* het; *Bdnf* cKO,  $P = 0.1530$ ,  $t = 1.684$ ; control vs. *Pten* cKO,  $P < 0.0001$ ,  $t = 55.87$ ; *Pten* cKO vs. *Pten* cKO; *Bdnf* cKO,  $P = 0.0012$ ,  $t = 6.661$ , d.f. = 13,  $F = 1,895$ ) and exhibit a larger MBP<sup>+</sup> myelinated area (d, e: 7 weeks, control vs. *Pten* het; *Bdnf* cKO,  $P = 0.4886$ ,  $t = 0.7619$ ; control vs. *Pten* cKO,  $P = 0.0085$ ,  $t = 4.196$ ; *Pten* cKO vs. *Pten* cKO; *Bdnf* cKO,  $P = 0.0024$ ,  $t = 5.021$ ,  $F = 40.64$ , d.f. = 13; 10 weeks, control vs. *Pten* het; *Bdnf* cKO,  $P = 0.3938$ ,  $t = 0.9547$ ; control vs. *Pten* cKO,  $P = 0.0039$ ,  $t = 5.979$ ; *Pten* cKO vs. *Pten* cKO; *Bdnf* cKO,  $P = 0.0476$ ,  $t = 2.611$ ,  $F = 23.02$ , d.f. = 12) compared to single *Pten* mutants (quantitated on parasagittal sections of the cerebellar vermis;  $n = 3–4$  mice per age and genotype). (f) EM view of *Pten*; *Bdnf* double mutants and single *Pten* mutants showed that axon sizes are unchanged, whether myelinated ( $P = 0.4339$ ,  $t = 0.869$ , d.f. = 4) or unmyelinated Pf ( $P = 0.5558$ ,  $t = 0.642$ , d.f. = 4; age 10 weeks;  $n = 3$  mice per genotype). (g, h) G-ratio analysis of ML myelin in *Pten* single mutants and *Pten*; *Bdnf* double mutants ( $P = 0.0259$ ,  $t = 3.454$ , d.f. = 4; 250–490 myelinated Pf axons per animal;  $n = 3$  mice per genotype; age 10 weeks). (i) BrdU administered from P25 to P45 and histology performed 4 d later. The number of BrdU<sup>+</sup>Olig2<sup>+</sup> cells is higher in *Pten*; *Bdnf* double mutants compared to *Pten* single mutants (control vs. *Pten* het; *Bdnf* cKO,  $P = 0.0419$ ,  $t = 2.74$ ; control vs. *Pten* cKO,  $P < 0.0001$ ,  $t = 16.53$ ; *Pten* cKO vs. *Pten* cKO; *Bdnf* cKO,  $P = 0.0426$ ,  $t = 2.565$ ,  $F = 56.01$ , d.f. = 13; quantified in the ML of parasagittal sections of the cerebellar vermis;  $n = 3–4$  mice per genotype). Data are mean  $\pm$  s.e.m.; n.s., not significant; \* $P < 0.05$ , \*\* $P < 0.01$ , \*\*\* $P < 0.001$ ; two-tailed unpaired Student's *t*-test in f and h or one-way ANOVA followed by Bonferroni test in c, e and i. Images in a, b and d are representative of  $\geq 3$  similar experiments.



a critical period in development at which the identified PI(3,4,5)P<sub>3</sub>-dependent neuronal program can trigger myelination.

Searching for promyelinating factors, we laser-captured stripes of GL from cryosections of 3-month-old mutants and controls for transcriptome analyses (Fig. 3a). A resulting list of candidate genes upregulated in *Pten* cKO was further selected by annotation (Supplementary Table 1) and validated with reverse transcription quantitative real-time PCR (qPCR; data not shown).

To confirm the significance of these findings *in vivo*, we tested Bdnf (ref. 9), reasoning that its inactivation might affect *de novo* myelination. Unexpectedly, *Tg(mα6)-Cre;Pten<sup>loxP/loxP</sup>;Bdnf<sup>loxP/loxP</sup>* mice (hereafter termed *Pten;Bdnf* double mutants) exhibited a higher (not lower) number of oligodendrocytes in the ML compared to *Pten* single mutants (Fig. 3b,c). Immunostaining also showed that the myelinated area of the ML was not smaller but larger (Fig. 3d,e). By EM, we confirmed that Pf axon calibers were as enlarged in *Pten;Bdnf* double mutants as in *Pten* single mutants (Fig. 3f). However, g-ratio analysis showed that myelin was thinner in *Pten;Bdnf* double mutants than in *Pten* single mutants (Fig. 3g,h). Thus, in the absence of Bdnf, mutant oligodendrocytes are more numerous in the ML, but each fiber is only thinly ensheathed. Most likely, OPCs respond to either proliferation or differentiation signals but not to both. In the absence of Bdnf (a differentiation signal), the weight of proliferation signals might increase, driving the number of OPCs up. However, differentiation signals may compensate later and turn all OPCs into oligodendrocytes, explaining a seemingly paradoxical result.

To test this hypothesis directly, we compared OPC proliferation in *Pten;Bdnf* double mutants and single mutants at 7 weeks of age, following BrdU labeling (P25–P45). Indeed, double mutants showed 34% more BrdU-labeled (Olig2<sup>+</sup>) OPCs in the ML than *Pten* single mutants (Fig. 3i). Unexpectedly, the lack of Bdnf even promoted proliferation of OPCs in heterozygous *Pten* mutants compared to controls (Fig. 3i). This suggests that Bdnf helps control the number of OPCs, which are likely to turn over in the absence of other myelination-promoting factors. For comparison, *Nrg1* (essential for myelination by Schwann cells<sup>1</sup>) revealed no such effects on *de novo* myelination in *Tg(mα6)-Cre;Pten<sup>loxP/loxP</sup>;Nrg1<sup>loxP/loxP</sup>* mice (Supplementary Fig. 7).

Because of the complexity of Bdnf effects *in vivo*, we studied other candidate factors (emerging from our screen) in primary oligodendrocyte cultures and in myelinating neuron–oligodendrocyte cocultures, using recombinant proteins to test their role in OPC proliferation, differentiation and/or myelination. Indeed, Fgf1 stimulated proliferation of OPCs (Supplementary Figs. 8a–d and 9, and Supplementary Note). Activin-A, the biologically active dimer of two inhibin beta A (*Inhba*) subunits, emerged as a differentiation factor<sup>10</sup> that required MAPK (ERK1 and ERK2) but not PI3K or SMAD3 (Supplementary Fig. 8e–i and Supplementary Note) to be effective. Pleiotrophin, *Tmsb4x* and *Timp3* also stimulated *in vitro* myelination (Supplementary Fig. 8g,h and Supplementary Note).

Increased axon size was further associated with upregulated expression of several other genes. Some mRNAs encoded secreted proteins already associated with oligodendrocyte development such as Bdnf, *Vegfc* and *Tmsb4x* (refs. 9,11,12). Other factors, including *Fstl1*, *Igfbp-4*, *Dkk-3*, *Apcdd1* and *Sfrp4*, are known antagonists of Wnt and Bmp signaling<sup>13,14</sup>, inhibit oligodendrocyte differentiation<sup>15</sup>. Modulators of IGF signaling and metalloproteinases (MMP17, *Adamts1*) were also upregulated, the latter degrading inhibitors of remyelination. We note that membrane proteins not transcriptionally upregulated may also increase in abundance when axons grow radially.

Taken together, we have identified an upstream neuronal ‘switch’, the PI3K–AKT1–mTOR pathway, which was sufficient to trigger the entire program of radial axonal growth<sup>16</sup>, recruitment of OPCs and progressive myelination in the CNS. Axonal specializations, such as the clustering of Caspr at paranodal junctions, were part of this neuronal myelination program. Myelination was triggered by a combination of both the increase of axon caliber (> 0.25 μm) and the induced expression of numerous promyelinating factors. Axon caliber poses a critical threshold for myelination in the peripheral and central nervous system, as recently shown for cultured oligodendrocytes myelinating carbon nanofibers<sup>17</sup>. However, CNS myelination begins with OPC recruitment and expansion, followed by oligodendrocyte differentiation, all without axonal contact. Only once differentiated oligodendrocytes physically engulf axons is the minimum caliber required to allow membrane wrapping. Schwann cells, in contrast, are always physically associated with axons and stimulated by a key membrane-bound growth factor, *Nrg1* type III (ref. 1).

Downstream of the neuronal myelination switch, not all promyelinating factors are of neuronal origin, in line with previous findings<sup>10</sup>. We also identified immune modulatory factors that were upregulated, such as *Nts* (neurotensin) and *Ninj1* (*ninjurin 1*), previously implicated in immune cell migration<sup>18,19</sup>. Since moderate changes in *Iba1*, *Mac-3* and GFAP expression were detected in the mutant ML (Supplementary Fig. 10a–c), we asked whether non-neuronal cells responded to *Pten* deletion in *Nex-CreERT2;Pten<sup>loxP/loxP</sup>* mutants (which showed only 4% GC recombination but significant myelination). Here, no ‘gliosis’ markers were detected in ML and GL, even 28 weeks after recombination (Supplementary Fig. 11). Thus, *de novo* myelination was not dependent on any form of gliosis.

Moreover, several factors were expressed in endothelial cells (Supplementary Table 1) and CD31 immunostaining showed increased angiogenesis in the mutant GL (Supplementary Fig. 10d). This is in line with the recently identified coupling of myelination to angiogenesis<sup>20</sup>.

Notably, not all *Pten* mutant neurons were myelinated, as evidenced by hippocampal neurons in *Nex-CreERT2;Pten<sup>loxP/loxP</sup>* mutants. Despite efficient recombination of hippocampal CA3 neurons<sup>8</sup> and significant increase in the size of neuronal somata ( $P = 0.0005$ ,  $t = 10.18$ , d.f. = 4), Schaffer collateral axons remained unmyelinated (Supplementary Fig. 12). This suggests a role of inhibitory signals that may ‘protect’ axons from myelination, which would interfere with sprouting and neuronal plasticity in the adult. However, we have no formal proof that all axons were sufficiently enlarged, as EM sections did not allow us to positively identify the Schaffer collaterals.

In multiple sclerosis, lesioned areas fail to repair, presumably because of a poor balance of myelination promoting and inhibiting cues. Significant progress has been made in identifying small molecules targeting OPCs and oligodendrocytes in remyelination. Our data suggest that neurons should also be considered as therapeutic targets when searching for myelin repair strategies.

## METHODS

Methods, including statements of data availability and any associated accession codes and references, are available in the online version of the paper.

**Accession codes.** GEO: GSE80966.

*Note: Any Supplementary Information and Source Data files are available in the online version of the paper.*

## ACKNOWLEDGMENTS

We are grateful to A. Fahrenholz, U. Bode, C. Stuenkel and H.N. Hidaji for technical support and thank T. Ruhwedel and W. Moebius for help with electron microscopy. We thank U. Fünfschilling and L. Reichardt (University of California, San Francisco) for *Tg(mα6)-Cre* mice, H. Wu (University of California at Los Angeles School of Medicine) for *Pten loxP*-flanked mice, M. Sendtner (University of Würzburg) for *Bdnf loxP*-flanked mice, C. Birchmeier (Max-Delbrück-Center for Molecular Medicine, Berlin) for *Nrg1 loxP*-flanked mice, P. Soriano (Icahn School of Medicine at Mount Sinai, New York) for *Rosa26-lacZ* reporter mice, J. Trotter (Johannes Gutenberg University, Mainz) for *Ng2-EYFP* mutants, F. Kirchhoff (University of Saarland, Homburg) for *Plp1-DsRed* transgenic mice, B. Emery (Oregon Health and Science University, Portland) for a *Myrf* *in situ* hybridization probe, and S. Ghandour (University of Strasbourg) and J. Alberta (Dana-Farber Cancer Institute, Boston) for primary antibodies. This work was supported by grants from the German Research Foundation (KFO241 to M.J.R., GO 2463/1-1 to S.G. and SPP-1172 to K.-A.N.) and by an ERC Advanced grant to K.-A.N.

## AUTHOR CONTRIBUTIONS

S.G. and K.-A.N. developed the study concept and design. A.P., B.W., O.Y., J.M.E., K.K. and G.L.W. performed immunoblotting, immunohistochemistry, cell culture analyses and electron microscopy under the supervision of S.G. K.Y. performed *in situ* hybridization. N.R. performed volume imaging under the supervision of M.T.-L. G.L.W. and S.P.W. performed laser-capture microdissection and subsequent microarray hybridization under the supervision of M.J.R. S.S. performed electrophysiological recordings under the supervision of R.T.K. A.A. generated *Nex-CreERT2* mutant mice. S.G., G.L.W., R.T.K. and K.-A.N. wrote the manuscript. All authors contributed to and approved the manuscript.

## COMPETING FINANCIAL INTERESTS

The authors declare no competing financial interests.

Reprints and permissions information is available online at <http://www.nature.com/reprints/index.html>.

1. Nave, K.A. & Salzer, J.L. *Curr. Opin. Neurobiol.* **16**, 492–500 (2006).
2. Brinkmann, B.G. *et al. Neuron* **59**, 581–595 (2008).
3. Stiles, B., Groszer, M., Wang, S., Jiao, J. & Wu, H. *Dev. Biol.* **273**, 175–184 (2004).
4. Fünfschilling, U. & Reichardt, L.F. *Genesis* **33**, 160–169 (2002).
5. Lesche, R. *et al. Genesis* **32**, 148–149 (2002).
6. Gibson, E.M. *et al. Science* **344**, 1252304 (2014).
7. Karram, K. *et al. Genesis* **46**, 743–757 (2008).
8. Agarwal, A. *et al. Cereb. Cortex* **22**, 1473–1486 (2012).
9. Xiao, J. *et al. Neurosignals* **18**, 186–202 (2010).
10. Miron, V.E. *et al. Nat. Neurosci.* **16**, 1211–1218 (2013).
11. Le Bras, B. *et al. Nat. Neurosci.* **9**, 340–348 (2006).
12. Santra, M. *et al. Glia* **60**, 1826–1838 (2012).
13. Cruciat, C.M. & Niehrs, C. *Cold Spring Harb. Perspect. Biol.* **5**, a015081 (2013).
14. Sylva, M., Moorman, A.F. & van den Hoff, M.J. *Birth Defects Res. C Embryo Today* **99**, 61–69 (2013).
15. He, L. & Lu, Q.R. *Neurosci. Bull.* **29**, 129–143 (2013).
16. Markus, A., Zhong, J. & Snider, W.D. *Neuron* **35**, 65–76 (2002).
17. Lee, S. *et al. Nat. Methods* **9**, 917–922 (2012).
18. Katsanos, G.S. *et al. Int. J. Immunopathol. Pharmacol.* **21**, 255–259 (2008).
19. Ifergan, I. *et al. Ann. Neurol.* **70**, 751–763 (2011).
20. Yuen, T.J. *et al. Cell* **158**, 383–396 (2014).

## ONLINE METHODS

**Mouse mutants.** All experiments were conducted according to the Lower Saxony State regulations for the use of experimental animals in Germany as approved by the Niedersächsische Landesamt für Verbraucherschutz und Lebensmittelsicherheit (LAVES) and according to UK government animal use regulations. Mice were housed in groups in individually ventilated cages under a 12:12 h light/dark cycle with access to food and water *ad libitum*. If not stated otherwise, for molecular, histological, electrophysiological, electron microscopic and biochemical experiments, female and male mice were included in the experiments and were randomly allocated to experimental groups according to age and genotype. All animal experiments were conducted in a single-blinded fashion toward the investigator. Inclusion/exclusion criteria were pre-established. Animals were excluded from the experiment when showing impaired health conditions not attributable to genotype or experiment or when the weight difference between the individual animal and the average group weight was larger than 10%. With respect to the outcome assessment, exclusion criteria were determined with Grubbs' test (ESD method), using the statistical software GraphPad (Prism). No animals or samples had to be excluded with these criteria in any of the experiments.

Mice mutant for *Pten*<sup>loxP/loxP</sup>, *Tg(mα6-Cre)B1LFR*, *Nex-CreERT2*, *Nrg1*<sup>loxP/loxP</sup>, *Bdnf*<sup>loxP/loxP</sup>, *Plp1-DsRed*, *Rosa26-lacZ* and *Ng2-EYFP* were genotyped as described<sup>4,5,7,8,21–24</sup>. *Tg(mα6-Cre)B1LFR*, *Nex-CreERT2*, *Nrg1*<sup>loxP/loxP</sup>, *Bdnf*<sup>loxP/loxP</sup>, *Plp1-DsRed*, *Rosa26-lacZ* and *Ng2-EYFP* mutants were on a C57BL/6N background, whereas *Pten*<sup>loxP/loxP</sup> mutants and thus all compound mutants harboring *Pten*<sup>loxP</sup> alleles were on a mixed C57BL/6N-SV129 background. For genotyping, genomic DNA was isolated from tail biopsies (InvisorbSpin Tissue Mini kit, Invitex) according to the manufacturer's directions and subjected to routine PCR methods using the following primers:

*Pten* sense: 5'-ACTCAAGGCAGGGATGAGC-3' and antisense: 5'-CAGAGTTAAGTTTTGAAGCAAG-3';

*Tg(mα6-Cre)B1LFR* sense: 5'-TAGAGCATTAGGGTGGGAG-3' and antisense: 5'-TGCCGCCTTTCAGGTGTGTCTTAC-3';

*Nrg1* sense: 5'-GCACCAAGTGGTTGCCATTGTTGCT-3' and antisense: 5'-TCCTTTGTGTGTGTTTCAGCACCG-3';

*Bdnf* sense: 5'-GTTGCGTAAGTCTGTGTCAGCTGTGC-3' and antisense: 5'-CAGACTCAGAGGGCATTGTATGGCTTG-3'

*Plp1-DsRed* sense: 5'-CGCCGACATCCCCGACTACAA-3' and antisense: 5'-GCGGCCCTACAGGAACAGGT-3';

*Rosa26-lacZ* sense: 5'-AAAGTCGCTCTGAGTTGTTAT-3' and antisense: 5'-GCGAAGAGTTTGTCTCAACC-3'; and

*Ng2-EYFP* sense: 5'-TGACCTTGGATTCTGAGC-3' and antisense: 5'-CGCTGAACCTTGTGGCCGTTTA-3'.

**BrdU labeling.** Mice received 5'-bromodeoxyuridine (BrdU, Sigma Aldrich) by daily intraperitoneal injections (50 μg/g of body weight) for 5, 10 or 20 consecutive days. Mice were killed for analysis 4 h or 4 d after the final injection.

**Histology and immunohistochemistry.** Mice were anaesthetized with Avertin (Sigma–Aldrich) and perfused with 15 ml of Hank's balanced salt solution (HBSS, PAA Laboratories, Pasching, Austria) followed by fixative (4% PFA, 0.1M Phosphate buffer, 0.5% NaCl). Paraffin sections of the brain (5 μm) were deparaffinized using xylene and isopropanol and rehydrated in a descending ethanol series. Antigen unmasking was performed by boiling for 10–40 min in citric buffer, pH 6, or Tris EDTA, pH 9. Sections were blocked in 20% goat serum in PBS/BSA for 1 h and incubated with primary antibodies in 5% goat serum in PBS/BSA for 2 h at 37 °C or overnight at 4 °C. Detection was performed using Alexa Fluor 488-, 555- and 633-conjugated secondary antibodies (1:1,000, Thermo Fisher Scientific, #A-28175, #A-11034, #A-21212, #A-21422, #A-27039 and #A-21094) and biotinylated secondary antibodies, followed by diaminobenzidine (DAB; LSAB2 Kit, Dako, #K0675; Vectastain Kit, Vector Laboratories, #BA-9400 and #PK-6100). Primary antibodies were directed against BrdU (1:200, Chemicon, #MAB3424), CAII (1:200, kindly provided by S. Ghandour, University of Strasbourg, PMID: 118210), calbindin (1:600, Sigma, #C9848), Caspr (1:100, NeuroMab, #75-001), CD31 (1:100, Dianova, #DIA-310), CNP (1:150, Sigma, #C5922), GABA<sub>A</sub> receptor α6 subunit (1:500, Chemicon, #AB5610), GFAP (1:200, Novocastra, #NCL-GFAP-GA5), Iba1 (1:1,000, Wako, #019-19741),

MBP (1:200, Covance, #SMI-94R); Na<sub>v</sub>1.6 (1:500, Alomone Labs, #ASC-009); NeuN (1:200, Chemicon, #MAB377); Olig2 (1:200, kindly provided by J. Alberta, Dana-Farber Cancer Institute, Boston, PMID: 15198128) and Mac-3 (1:500, BD Pharmingen, #553322). We also stained 5 μm microtome sections (Microm HM400) with hematoxylin–eosin (HE) to study cytoarchitecture. Myelinated fibers were visualized by Gallyas silver impregnation as described<sup>25</sup>. All images showing immunohistochemical analyses and stainings were successfully repeated at least three times. iDISCO whole-mount anti-CNP immunohistochemistry was performed according to the published protocol<sup>26</sup> on dissected cerebella from control and mutant animals. Monoclonal anti-CNP primary antibody (1:200, Sigma, #C5922) was used with 4 d incubation at 37 °C. Donkey anti-mouse Alexa Fluor 647-conjugated secondary antibody (1:1,000, Life Technologies, #A-31571) was used for 4 d at 37 °C. After clearing, samples were imaged on a LaVision Ultramicroscope II with a 2×0.5-NA objective and on an Olympus FV-1000 two-photon microscope with a 25×1.05-NA water-immersion objective and a laser tuned at 820 nm. Image stacks were analyzed with Imaris 8.01 (Bitplane).

**In situ hybridization.** *In situ* hybridization was performed as described<sup>27</sup>. A *Myrf* probe corresponding to 941 bp from *Myrf* 3' UTR was kindly provided by B. Emery (Oregon Health and Science University, Portland).

**Electron microscopy.** Mice were anaesthetized with Avertin (Sigma–Aldrich) and perfused with 15 ml of Hanks balanced salt solution (HBSS, PAA laboratories, Pasching, Austria) followed by fixative (4% PFA, 0.1 M Phosphate buffer, 0.5% NaCl, 2.5% glutaraldehyde). At parasagittal plane, cerebellar lobule V was dissected, contrasted with 1% osmium tetroxide and embedded in epoxy resin. Semithin (0.5 mm) and ultrathin (50–60 nm) sections were cut using a microtome (RM 2155, Leica Microsystems, Wetzlar, Germany) with a diamond knife (Histo HI 4317, Diatome, Biel, Switzerland). Semithin sections were stained with azure-II–methylene blue for 1 min at 60 °C. Ultrathin sections were stained with 2% uranyl acetate (30 min) and 1% lead citrate solution (12 min) and analyzed using a LEO EM912AB electron microscope (Carl Zeiss NTS, Oberkochen, Germany). Images were taken with an on-axis 2,048 × 2,048 CCD camera (Proscan, Scheuring, Germany).

**Electrophysiology.** Parasagittal cerebellar slices (225 μm) were cut using a vibrating blade microtome (Leica VT1200S) from P7–P100 *Ng2-EYFP*<sup>+/-</sup>; *Tg(mα6-Cre);Pten*<sup>loxP/loxP</sup> mice (mutants) and *Ng2-EYFP*<sup>+/-</sup>; *Pten*<sup>loxP/loxP</sup> mice (controls), killed by cervical dislocation in accordance with UK government animal use regulations. After dissection, the brain was placed in a cooled (~1 °C) oxygenated (95% O<sub>2</sub>–5% CO<sub>2</sub>) Krebs solution containing (in mM): 126 NaCl, 24 NaHCO<sub>3</sub>, 1 NaH<sub>2</sub>PO<sub>4</sub>, 2.5 KCl, 2.5 CaCl<sub>2</sub>, 2 MgCl<sub>2</sub>, 10 D-glucose (pH 7.4). In addition, kynurenic acid was included in order to block glutamate receptors, which might be activated during the dissection procedure and cause cell damage. During experiments, slices were superfused at 22 ± 1 °C with HEPES-buffered external solution containing (in mM): 144 NaCl, 2.5 KCl, 10 HEPES, 1 NaH<sub>2</sub>PO<sub>4</sub>, 2.5 CaCl<sub>2</sub>, 10 glucose, 0.1 glycine (to coactivate NMDA receptors), 0.005 strychnine (to block glycine receptors), pH set to 7.4 with NaOH, bubbled with 100% O<sub>2</sub>. OPCs were identified by EYFP expression and whole-cell voltage clamped. Recording electrodes had a resistance of 5–9 MΩ when filled with an internal solution comprising (in mM): 130 κ-gluconate, 4 NaCl, 0.5 CaCl<sub>2</sub>, 10 HEPES, 10 BAPTA, 4 MgATP, 0.5 Na<sub>2</sub>GTP, 2 K-Lucifer yellow, pH set to 7.3 with KOH; the uncompensated series resistance was 40 ± 1 MΩ, and electrode junction potentials (–14 mV) were compensated for. A Multiclamp 700B (Molecular Devices) was used for voltage clamp data acquisition. Data were sampled at 50 kHz and filtered at 10 kHz using pClamp10.3 (Molecular Devices).

**Synaptic current analysis.** A synaptic current was defined to occur if its amplitude was greater than twice the s.d. of the baseline current noise and its 10–90% decay time was longer than its rise time. Events were detected and analyzed with pClamp 10.3 (Molecular Devices) and the Strathclyde Electrophysiology Software package WinEDR V3.3.7 WinWCP V4.6.2.

**Laser-capture microdissection, RNA isolation and linear amplification, and microarray hybridization.** Mice were killed at 3 months of age by cervical dislocation; whole brains were dissected and frozen on dry ice, protected with parafilm and stored at –80 °C. Serial coronal cryosections (20 μm) were

prepared using a Leica CM3000 Cryostat, mounted on polyethylene naphthalate membrane frame slides (Arcturus), stained with thionin and dried in an ascending ethanol/xylene series. For laser-capture microdissection (LCM), a Veritas Microdissection System (Arcturus) was used, with slides mounted and stained the same day. Cerebellar GL were dissected by ultraviolet laser (laser power set to 3.2–4.2) and attached to CapSure LCM caps using an infrared laser (power set to 80%). Caps were collected in 0.5 ml Eppendorf tubes containing 100  $\mu$ l of RNeasy Lysis Buffer (Qiagen) and stored at  $-80^{\circ}\text{C}$ . Total RNA was isolated from LCM tissue using the Micro RNeasy Kit (Qiagen) according to the instructions of the manufacturer, except that RNA was eluted from the column with 10  $\mu$ l of water followed by precipitation with NaAcetate (pH 5.2, f.c. 0.3 M) and PelletPaint (Novagen) as carrier. Two-round amplification and biotin labeling, hybridization to mouse MOE230A 2.0 Genechip arrays (Affymetrix), washing and scanning was conducted essentially as described<sup>28</sup> with three biological replicates for each genotype. Data analysis was performed using Genomics Suite (Partek Inc.). Raw data were normalized using the RMA algorithm, and differentially expressed genes were identified with ANOVA according to the workflow suggested by the manufacturer (Partek Inc.). Differentially expressed genes with signal intensities in mutants > controls were selected with > 1.4-fold change and adjusted *P*-values < 0.05.

**RNA isolation, cDNA synthesis and qRT-PCR.** Total RNA was isolated from LCM tissue using the Transcriptor High Fidelity Kit (Roche) according to the instructions of the manufacturer. cDNA was synthesized using a mixture of random nonamer primers, anchored poly-dT primers and SuperScript III RNase H reverse transcriptase (Invitrogen) according to the instructions of the manufacturer. qRT-PCR was performed using SYBR green master mix (Applied Biosystems) and a 7500 Fast Real-Time PCR System (Applied Biosystems). Primers were designed using the Roche Universal ProbeLibrary website (<http://qpcr.probefinder.com>). Primer sequences are available upon request. Relative mRNA concentrations were normalized to Actin and Atp5b. Data were analyzed using qBase software version 1.3.5 (Center for Medical Genetics, Ghent University, Ghent, Belgium).

**Mixed myelinating cocultures from mouse spinal cord.** Wild-type C57BL/6N mice were time-mated, with the day of plugging denoted as embryonic day 0.5 (E0.5), and embryos were collected on embryonic day 13.5 (E13.5). The spinal cord was dissected and was dissociated mechanically and enzymatically (0.25% trypsin, Invitrogen). Enzymatic activity was stopped by the addition of plating medium (50% DMEM, 25% horse serum, 25% Hank's balanced salt solution without  $\text{Ca}^{2+}$  and  $\text{Mg}^{2+}$ ) containing 2.5  $\mu\text{g}/\text{ml}$  DNase I. Cells were dissociated into a single cell suspension by triturating through 20- and 23-gauge needles (4 and 2 times, respectively) and spun at 800 rpm for 5 min. The pellet was resuspended in plating medium. Dissociated spinal cord cells were initially plated at a density of 150,000 cells/100  $\mu\text{l}$  onto poly-L-lysine (PLL, in boric acid buffer, pH 8.4)-coated coverslips, which were then placed into a 35-mm Petri dish. The cells were left to attach for 2–3 h, after which 150  $\mu\text{l}$  of plating medium and 500  $\mu\text{l}$  of differentiation medium was added. This medium contained DMEM (4,500 mg/L glucose), 10 mg/ml biotin, 0.5% hormone mixture (1 mg/mL apotransferrin, 20 mM putrescine, 4  $\mu\text{M}$  progesterone and 6  $\mu\text{M}$  selenium), 50 nM hydrocortisone and 10  $\mu\text{g}/\text{ml}$  insulin (all reagents from Sigma). Cultures were maintained by replacing half of the medium with fresh medium three times per week. After 12 d in culture, cells were fed with differentiation medium with (or without) recombinant human PDGF (100 ng/ml), SPARCL1 (10 ng/ml), VEGFC (100 ng/ml), FGF1 (100 ng/ml), PTN (10 ng/ml), TIMP3 (100 ng/ml), TMSB4X (50 ng/ml) or Activin A (100 ng/ml) and reduced concentration of insulin (0.2  $\mu\text{g}/\text{ml}$ ). Cultures were maintained for up to 25 days in a humidified atmosphere of 5%  $\text{CO}_2$  at 37  $^{\circ}\text{C}$ .

**Mixed primary oligodendrocyte cultures.** Mixed primary oligodendrocyte cultures were prepared from (7 pooled) spinal cords of P4 mouse pups. Tissue chunks were incubated in 5 ml papain (200 U) in papain buffer plus L-cysteine for 1 h at  $\sim 35^{\circ}\text{C}$  with constant gassing (95% oxygen and 5% carbon dioxide). The papain reaction was stopped with plating medium (30% horse serum in DMEM) containing 2.5  $\mu\text{g}/\text{ml}$  DNase I. Cells were dissociated into a single cell suspension by triturating through 20- and 23-gauge needles (4 and 2 times, respectively), spun at 800 rpm for 5 min, and the pellet was resuspended in plating

medium. Cells were plated at a concentration of 80,000 cells/100  $\mu\text{l}$  plating medium onto PLL-coated, 11-mm diameter glass coverslips, in 35-mm diameter Petri dishes (2 coverslips/dish). Two hours later, differentiation medium containing DMEM (4,500 mg/L glucose), 10 ng/ml biotin, 0.5% hormone mixture (1 mg/mL apotransferrin, 20 mM putrescine, 4  $\mu\text{M}$  progesterone and 6  $\mu\text{M}$  selenium), 50 nM hydrocortisone and 10  $\mu\text{g}/\text{ml}$  insulin (all reagents from Sigma) was added to each 35-mm Petri dish to yield a mix of 50% plating medium: 50% differentiation medium. The following day all medium and myelin debris was removed from the coverslips by rinsing briefly in medium, and fresh differentiation medium was added to each 35-mm Petri dish, with or without human recombinant forms of KLOTHO (400 ng/ml), PTN (10 ng/ml), TIMP3 (100 ng/ml) or Activin A (100 ng/ml). Cells were fed every second day by replacing half the medium with fresh differentiation medium, including the recombinant proteins. Cultures were maintained for 3 and 5 d in a humidified atmosphere of 5%  $\text{CO}_2$  at 37  $^{\circ}\text{C}$ .

**Recombinant proteins.** Human recombinant proteins were SPARCL1, VEGFC, KLOTHO, TIMP3 and Activin A (R&D Systems), PDGF and PTN (Sigma Aldrich), TMSB4X (Novus Biologicals) and FGFL (Invitrogen). Recombinant proteins were dissolved in  $\text{ddH}_2\text{O}$ . Individual aliquots were thawed only once and diluted in cell culture medium immediately before use. PI3K inhibitor LY294002 and MEK1/2 inhibitor UO126 were from Cell Signaling Technology; SMAD3 inhibitor SIS3 was from Calbiochem.

**Immunocytochemistry.** Cells were fixed with 4% PFA for 5 min at 37  $^{\circ}\text{C}$ . After fixation, cultures were washed in PBS three times, permeabilized with ice-cold methanol for 5 min and blocked in blocking buffer (2% fish skin gelatin, 2% FCS, 2% BSA in PBS) for 60 min. Primary antibodies (diluted in 10% blocking buffer) were directed against GFAP (1:200, Novocastra, #NCL-GFAP-GA5), KI-67 (1:10, Dako, #M7249), MBP (1:200, Covance, #SMI-94R), Olig2 (1:200, kindly provided by J. Alberta, Dana-Farber Cancer Institute, Boston, PMID: 15198128), SMI31 (1:1,000, Covance, #SMI-31P) and APC-CC1 (1:100, Calbiochem, #OP80) and incubated overnight at 4  $^{\circ}\text{C}$ . Coverslips were washed in PBS three times. Corresponding secondary Alexa Fluor 488-, 555- and 633-conjugated antibodies (1:1,000, Thermo Fisher Scientific, #A-28175, #A-21422, #A-27039 and #A-21094) were diluted in 10% blocking buffer and added for 1 h. Coverslips were washed in  $\text{ddH}_2\text{O}$  three times and mounted in Aqua-Poly/Mount (Polysciences).

**Morphometry.** Digitized overlapping light microscopic images (20 $\times$ ) were fused to a continuous image of a complete parasagittal cerebellum (Lateral, 0.12 mm) using Zeiss Zen software and analyzed for absolute numbers of CNP<sup>+</sup>, CAII<sup>+</sup>, Olig2<sup>+</sup>, Iba1<sup>+</sup>, Mac-3<sup>+</sup> and BrdU<sup>+</sup> cells. The number of Iba1<sup>+</sup> and Mac-3<sup>+</sup> cells were normalized to the areas of ML and GL, respectively. Endothelial cells positive for CD31 were traced with ImageJ and normalized to the area of the ML. To quantify MBP<sup>+</sup> and GFAP<sup>+</sup> areas, two ImageJ plugins for semiautomated analysis were implemented ([http://www1.em.mpg.de/Goebbels2016\\_MBP](http://www1.em.mpg.de/Goebbels2016_MBP) and [http://www1.em.mpg.de/Goebbels2016\\_GFAP](http://www1.em.mpg.de/Goebbels2016_GFAP)). Average diameter of hippocampal CA3 neuronal cell bodies of *Nex-CreERT2;Pten<sup>loxP/loxP</sup>* mice was determined by using ImageJ software. Two independent sections per mouse and staining were quantified. In cell culture experiments, the differentiation and proliferation state of oligodendrocyte lineage cells was analyzed within the given fields of 11 randomly taken images (20 $\times$ ) per coverslip (mixed myelinating cultures: myelination assay, 3–11 independent experiments with 2 coverslips per condition; proliferation assay, 3–11 independent experiments with 1 coverslip per condition; mixed primary oligodendrocyte cultures: 3–5 independent experiments with 2 coverslips per condition). For quantitative assessment of *in vitro* myelination, a 'myelination index' was calculated by dividing the MBP<sup>+</sup> area (as identified by generating a 'mask' outlining the myelin sheaths; ImageJ plugin: [http://www1.em.mpg.de/Goebbels2016\\_CoCultureMBP](http://www1.em.mpg.de/Goebbels2016_CoCultureMBP)) by the axonal area (Smi31<sup>+</sup> axons; ImageJ plugin: [http://www1.em.mpg.de/Goebbels2016\\_CoCultureSmi31](http://www1.em.mpg.de/Goebbels2016_CoCultureSmi31)). For the proliferation assay, the percentage of semiautomatically quantified Olig2<sup>+</sup> cells was determined in relation to all DAPI<sup>+</sup> cells (Olig2; ImageJ plugin: [http://www1.em.mpg.de/Goebbels2016\\_CoCultureOlig2](http://www1.em.mpg.de/Goebbels2016_CoCultureOlig2); DAPI; ImageJ plugin: [http://www1.em.mpg.de/Goebbels2016\\_CoCultureDapi](http://www1.em.mpg.de/Goebbels2016_CoCultureDapi)) and the number of Ki67<sup>+</sup>Olig2<sup>+</sup> cells was set in relation to the total number of Olig2<sup>+</sup> cells. For the differentiation assay, the percentage of postmitotic oligodendrocytes was determined by quantifying and dividing the numbers of CCI1<sup>+</sup> cells by the total

number of Olig2<sup>+</sup> oligodendrocyte lineage cells. All analyses were performed in a single-blinded fashion toward the investigator, who was unaware of the treatment regimen.

**G-ratio measurement.** Digitized images (magnification 7,000×) of ultrathin cerebellum lobe 5 sections were used to determine the numbers of myelinated axons, axon calibers and g-ratios (> 100 randomly chosen myelinated axons in the ML). G-ratios were determined by dividing axon diameter by the diameter of the entire fiber (Fig. 1k) or by dividing the inner myelin diameter by the diameter of the entire fiber (Fig. 3g and Supplementary Fig. 7c). Quantitations were performed from ≥ 3 age-matched male mice per genotype and age.

**Protein analysis.** Cerebellum lysates were homogenized in lysis buffer (50 mM HEPES, pH 7.5, 150 mM NaCl, 1.5 mM MgCl<sub>2</sub>, 5 mM EGTA, 10% glycerol, 1% Triton X-100, 2 mM Na<sub>3</sub>VO<sub>4</sub>) containing phosphatase (PhosSTOP Inhibitor Cocktail, Roche, Basel, Switzerland) and protease (Complete tablets, Roche, Basel, Switzerland) inhibitors using an Ultraturax (T8, Ika, Staufen, Germany) at its highest settings (30–60 s). After incubation for 15 min on ice, insoluble material was removed by centrifugation at 16,000g at 4 °C for 15 min. For western blot analysis, 10 μg of protein lysate was size-separated on 12% of SDS-polyacrylamide gels and blotted onto PVDF membranes (HybondTM-P, Amersham Biosciences, UK) by Bio-Rad western blotting. Membranes were blocked in 5% milk powder (in PBS) for 1 h at room temperature (20–25 °C). Primary antibodies were directed against p-AKT1 (Cell Signaling, mRb, 1:1,000, #4060), AKT1 (Cell Signaling, mRb, 1:1,000, #4691), PTEN (Cell Signaling, mRb, 1:1,000, #9188), p-GSK3β (Cell Signaling, mRb, 1:1,000, #9336), p-mTOR (Cell Signaling, mRb, 1:1,000, #5536), p-S6 (Cell Signaling, mRb, 1:1,000, #4858) and Actin (Sigma-Aldrich, mM, 1:1,000, #A3853). Antibodies were diluted in blocking buffer and incubated overnight at 4 °C. Membranes were washed 3 times for 10 min each time in TBS-T buffer (50 mM Tris-HCl, pH 7.4, 150 mM NaCl and 0.05% Tween-20), followed by an incubation with horseradish-peroxidase-conjugated secondary antibodies (1:5,000, Dianova, #111-035-003 and #115-035-003). After three more washings with TBS-T buffer, immunoreactive proteins were detected with an enhanced chemiluminescence kit (Western LightningTM, Westernblot Chemiluminescence Reagent Plus, PerkinElmer Life Sciences, Waltham, MA) according to the manufacturer's instructions.

**Statistical analysis.** For power analysis we used G\*Power Version 3.1.7 software. Power analyses were performed before conducting experiments (a priori). Adequate power (1 – β) was defined as ≥ 80% and the α as 5%. The sample size was calculated with the following prespecified effect sizes:

1. mRNA expression analysis: effect size *d* of approximately 2.5 (estimated mean difference of 50% and s.d. of 15%).
2. Analysis of mature oligodendrocyte numbers in GL (effect size *d* of approximately 3.5, estimated mean difference of 30% and s.d. of 10%), ML (effect size *d* of approximately 6.5, estimated mean difference of 400% and s.d. of 30%) and myelinated areas in the MLs of controls and *Pten* mutants (effect size *d* of approximately 6.0, estimated mean difference of 170% and s.d. of 40%).
3. Proliferation analysis of oligodendrocyte lineage cells: effect size *d* of approximately 9.0 (estimated mean difference of 330% and s.d. of 15%).
4. *In vivo* analysis of candidate genes: analysis of mature oligodendrocyte numbers: effect size *d* of approximately 5.5 (estimated mean difference of 30% and s.d. of 15%); analysis of myelinated area: effect size *d* of approximately 4.0 (estimated mean difference of 30% and s.d. of 13%); proliferation analysis of oligodendrocyte lineage cells: effect size *d* of approximately 3.5 (estimated mean difference of 20% and s.d. of 10%); analysis of myelinated (effect size *d* of approximately 2.6 (estimated mean difference of 20% and s.d. of 13%)) and unmyelinated Pf axon diameters

(effect size *d* of approximately 1.5 (estimated mean difference of 15% and s.d. of 13%)); and g-ratio analysis: effect size *d* of approximately 4.5 (estimated mean difference of 6% and s.d. of 2%).

5. Microglia (ML: Effect size *d* of approximately 4.7, estimated mean difference of 100% and s.d. of 20%; GL: effect size *d* of approximately 1.2, estimated mean difference of 10% and s.d. of 5%), astrocytes (ML: effect size *d* of approximately 4.0, estimated mean difference of 150% and s.d. of 15%; GL: effect size *d* of approximately 1.3, estimated mean difference of 10% and s.d. of 5%) and vascular endothelia cells (effect size *d* of approximately 3.7, estimated mean difference of 40% and s.d. of 15%) in *Pten* mutant mice.
6. Microglia (ML: effect size *d* of approximately 1.0, estimated mean difference of 10% and s.d. of 9%; GL: effect size *d* of approximately 1.3, estimated mean difference of 10% and s.d. of 7%) and astrocytes (ML: effect size *d* of approximately 1.2, estimated mean difference of 20% and s.d. of 15%; GL: effect size *d* of approximately 1.1, estimated mean difference of 10% and s.d. of 5%) in *NEX-CreERT2;Pten<sup>loxP/loxP</sup>* mice.
7. Average diameter of hippocampal CA3 neuronal cell bodies from *Nex-CreERT2;Pten<sup>loxP/loxP</sup>* mice: effect size *d* of approximately 12.0 (estimated mean difference of 25% and s.d. of 2%).
8. *In vitro* analysis of candidate factors: analysis of oligodendrocyte lineage cell numbers: effect size *d* of approximately 4.0 (estimated mean difference of 80% and s.d. of 30%); proliferation analysis: effect size *d* of approximately 2.3 (estimated mean difference of 60% and s.d. of 36%); myelination index: effect size *d* of approximately 2.0 (estimated mean difference of 65% and s.d. of 50%); and analysis of oligodendrocyte differentiation: effect size *d* of approximately 9.0 (estimated mean difference of 40% and s.d. of 10%).

For electrophysiology experiments, we determined the sample size using previous data distributions. Data are expressed as mean ± s.e.m. In order to select appropriate statistical tests, all data have been tested for normal distribution with a Kolmogorov-Smirnov test or Shapiro-Wilk test. For normally distributed data with comparable variances, we used two-tailed unpaired Student's *t*-tests and chi-squared tests to determine the statistical significance between two groups. For data not showing normal distribution or for which no normality test could be conducted, the nonparametric Wilcoxon matched-pairs test was applied. Data sets containing more than two groups were tested by ANOVA and Bonferroni *post hoc* tests. Analysis of covariance (ANCOVA) was used to analyze the differences between slopes of regression lines. Applied statistical tests are indicated in the respective figure legends. Statistical differences were considered significant when  $P < 0.05$  (\* $P < 0.05$ , \*\* $P < 0.01$ , \*\*\* $P < 0.001$ ) and tests and fitting of regression lines were performed using GraphPad (Prism) and MS Excel.

A **Supplementary Methods Checklist** is available.

**Data availability.** The following ImageJ plugins were used and can be freely accessed under the following URLs: [http://www1.em.mpg.de/Goebbels2016\\_MBP](http://www1.em.mpg.de/Goebbels2016_MBP), [http://www1.em.mpg.de/Goebbels2016\\_GFAP](http://www1.em.mpg.de/Goebbels2016_GFAP), [http://www1.em.mpg.de/Goebbels2016\\_CoCultureMBP](http://www1.em.mpg.de/Goebbels2016_CoCultureMBP), [http://www1.em.mpg.de/Goebbels2016\\_CoCultureSmi31](http://www1.em.mpg.de/Goebbels2016_CoCultureSmi31), [http://www1.em.mpg.de/Goebbels2016\\_CoCultureOlig2](http://www1.em.mpg.de/Goebbels2016_CoCultureOlig2) and [http://www1.em.mpg.de/Goebbels2016\\_CoCultureDapi](http://www1.em.mpg.de/Goebbels2016_CoCultureDapi).

21. Hirrlinger, P.G. *et al.* *Mol. Cell. Neurosci.* **30**, 291–303 (2005).
22. Li, L. *et al.* *Oncogene* **21**, 4900–4907 (2002).
23. Rauskolb, S. *et al.* *J. Neurosci.* **30**, 1739–1749 (2010).
24. Soriano, P. *Nat. Genet.* **21**, 70–71 (1999).
25. Lappe-Siefke, C. *et al.* *Nat. Genet.* **33**, 366–374 (2003).
26. Renier, N. *et al.* *Cell* **159**, 896–910 (2014).
27. Bormuth, I. *et al.* *J. Neurosci.* **33**, 641–651 (2013).
28. Rossner, M.J. *et al.* *J. Neurosci.* **26**, 9956–9966 (2006).